Contents lists available at ScienceDirect

Chemical Engineering Research and Design

journal homepage: www.elsevier.com/locate/cherd

A modelling approach to assessing the feasibility of the integration of power stations with steam electrolysers

*Mithila N. Manage, Eva Sorensen, Stefaan Simons, Dan J.L. Brett**

Department of Chemical Engineering, University College London, London WC1E 7JE, UK

ABSTRACT

Hydrogen, combined with fuel cell technology, is an option for reducing our reliance on hydrocarbon-based fuels. Solid oxide electrolyser cells (SOECs) have been studied as a possible technology to produce hydrogen from steam. As the current global energy mix is heavily reliant on hydrocarbon-based fuels, utilising existing technologies such as coal fired power plants, combined with SOECs in an integrated system, may enable a path towards reducing carbon dioxide emissions as well as creating a way of introducing 'cleaner' fuel.

In this work, a steady state model of a SOEC was developed and used to assess the feasibility of using hot steam from a power plant as feed to a SOEC. The main objective was to study the ways of improving the SOEC efficiency. The most favourable feed for the SOEC was to extract steam prior to the intermediate pressure turbine, which showed SOEC efficiency improvement of 25% compared with conventional SOEC operation of heating water at 25 °C.

The thermoneutral point of 4644 A m^{-2} was shown to be a guide for assessing design and operation options with heat integration possibilities after this point. For scenarios of 7% steam extraction and a purely H_2 production plant, 250 MW (7500 kg h^{-1}) and 290 MW (8700 kg h^{-1}) H_2 can be produced with SOECs sized at 43,300 and 50,100 m^2, respectively.

Keywords: Solid oxide electrolyser; SOEC; Power plant; Hydrogen; Energy; Integrated system model

1. Introduction

Reducing carbon dioxide emissions has been the focus of many studies and has led to many changes in regulations within the energy sector. The combustion of hydrocarbon-based fuels for the production of power emits the largest proportion of CO_2 to the atmosphere. For example, 70% of CO_2 emissions from electricity producers in the UK were from coal fired power plants, which released 120 Mt of CO_2 in 2012 (Statistical Release, 2012). In order to reduce the reliance on hydrocarbon-based fuels, alternative fuels such as hydrogen are being studied. Hydrogen has the benefit of a large gravimetric energy density of 140.4 MJ kg^{-1} compared with 48.6, 53.6 and 18 MJ kg^{-1} for gasoline, natural gas and coal, respectively (Gupta, 2008; Manage et al., 2011; Natural Gas Reference Guidelines, 2012). Furthermore, hydrogen can be used to operate fuel cells, which produce electrical power via a highly efficient electrochemical route, with only water as the chemical by-product. This is beneficial for carbon emission reduction, as fuel cells can be used in place of traditional engines in vehicles.

Currently, H_2 is predominantly manufactured via steam methane reforming (SMR), with CO_2 as a by-product of the process (Manage et al., 2011). Although H_2 can be produced in large quantities from SMR, this process still relies on the availability of hydrocarbons and thus leads to the production of CO_2.

Solid oxide electrolyser cells (SOECs) are being studied as an alternative technology to be used for large-scale H_2

* *Corresponding author*. Tel.: +44 020 7679 3810.
E-mail address: d.brett@ucl.ac.uk (D.J.L. Brett).
Available online 7 August 2014
http://dx.doi.org/10.1016/j.cherd.2014.07.015

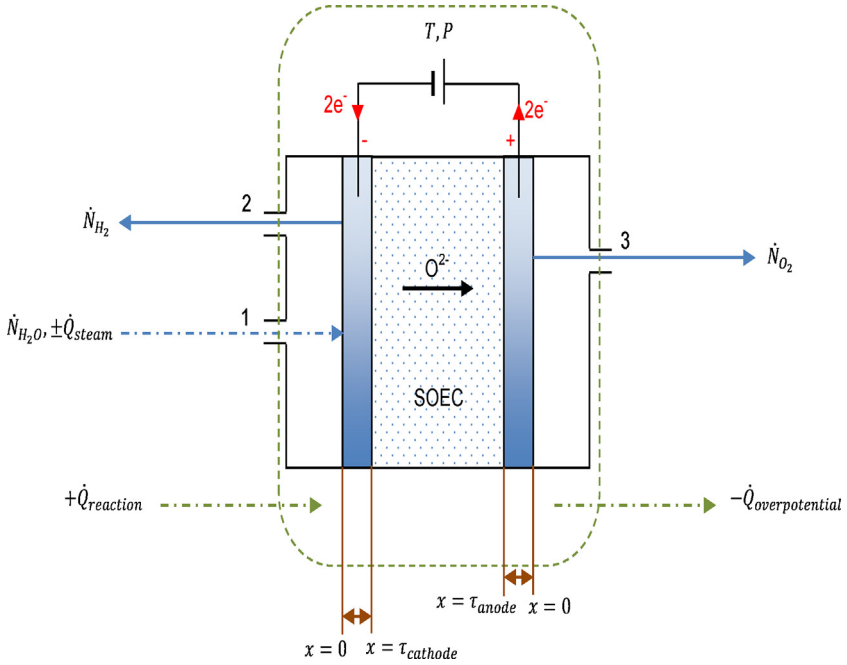

Fig. 1 – The operation of a planar solid oxide electrolyser cell.

production through the electrolysis of steam. The overall steam electrolysis reaction is as follows:

$$H_2O \rightarrow H_2 + \frac{1}{2}O_2 \quad (1)$$

SOECs operate as shown in Fig. 1, using steam as the reactant, which is separated into hydrogen and oxide ions at the cathode using electrical power. The oxide ions are transported through the electrolyte and form oxygen at the anode. The cathodes are made of a ceramic-metal mixture commonly known as a cermet to provide both electrical and ionic conductivity as well as being suitable for the high operating temperatures. The electrolyte is a highly ionic conducting ceramic to enable good oxide ion flow.

With the growing interest in SOECs, several models have been developed and shown in the literature (Udagawa et al., 2007; Cai et al., 2012; O'Brien et al., 2010; Perdikaris et al., 2010). As SOECs are currently only available at lab scale, modelling of cells and stacks has been carried out in order to estimate the behaviour of the cells at a range of scales and under varying conditions. SOECs are the reverse of solid oxide fuel cells (SOFCs), therefore the modelling of an electrolyser cell follows many of the same principles (Ni et al., 2006; Brisse et al., 2008). Most models have focused on considering main design and operating variables such as temperature, steam ratio, thickness of the cathode, anode and electrolyte, pressure and heating effects along the cell or stack (Ni et al., 2006; Udagawa et al., 2007; Cai et al., 2012; Laurencin et al., 2011).

Results presented in the literature have highlighted factors such as producing thin electrodes and electrolytes, in the range of 50 μm, which enables overpotentials to be kept to a minimum (Ni et al., 2006). The overpotentials refer to ohmic, activation and concentration resistances formed from electronic and ionic conduction, electro-kinetics and reactant and product flow limitations. Furthermore, reducing overpotentials enables greater SOEC efficiencies and reduces the temperature gradients that are generated through operation (Laurencin et al., 2011). The focus in the literature has mainly been on the understanding of the electrolysis process and the components within it. Variables such as steam temperature and composition have so far been a controlled variable, both experimentally (Kim-Lohsoontorn et al., 2011a; Kim et al., 2013) and computationally (Ni et al., 2006; Laurencin et al., 2011), and the energy required in order to produce steam for SOECs have not been considered as extensively. This study aims to assess the sensitivity of SOEC efficiency to variations in the temperature and pressure of the steam inlet. The integration of SOECs with a power station is then considered with a view to identifying the options and potential for efficiency optimisation.

2. Solid oxide electrolyser model

As SOECs are currently only available at lab scale, modelling of cells, stacks (a number of cells "stacked" together to form one unit) and more recently systems (several stacks combined with current technologies, e.g. wind turbines) have been carried out in order to estimate the behaviour of the cells under varying conditions. SOECs operate as the reverse of SOFCs; therefore modelling of an electrolyser cell effectively follows the same principles (Aguiar et al., 2004; Ni et al., 2006; Brisse et al., 2008). Many studies have shown that variables such as temperature, steam ratio and thickness of the components have significant effects on performance, with pressure having a relatively minor effect (Chan and Xia, 2002; Ni et al., 2006; Udagawa et al., 2007, 2008; Cai et al., 2012; Jensen et al., 2010; Laurencin et al., 2011).

Limited research has also been presented in literature examining systems-level operation and integration. Combining SOECs with nuclear technologies has been of great interest due to high quality heat available from gas cooled reactors. Hydrogen production efficiencies of 53% were reported with such a combination by Fujiwara et al. (2008), where the efficiency is related to the electrical requirements of the system. Thermal-to-hydrogen efficiency (heating value of hydrogen/total thermal input) of around 50%, with current density and temperature being influential variables, were seen by O'Brien et al. (2010).

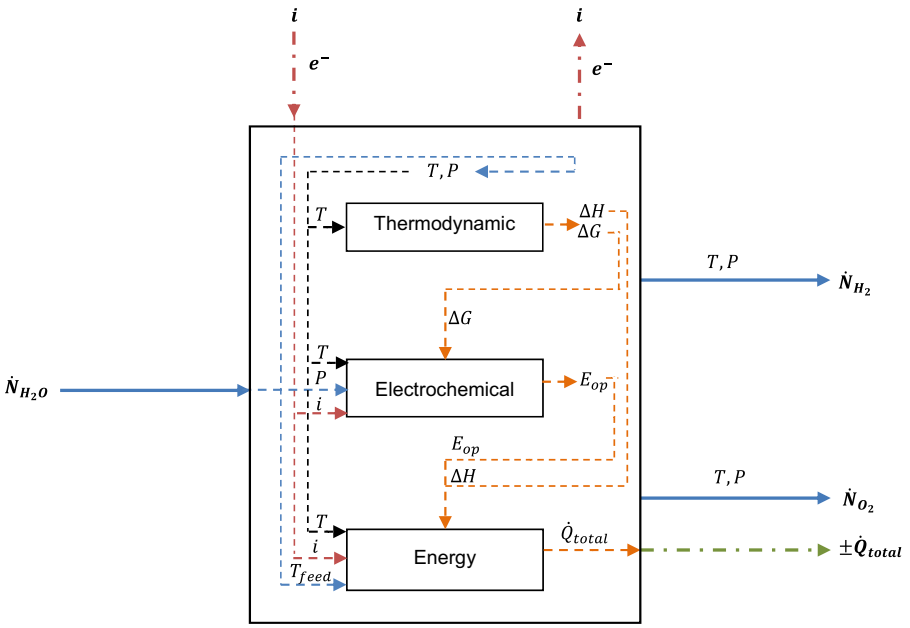

Fig. 2 – An overview of the inputs and outputs to the SOEC. The links between each section of the model in relation to physical inputs are shown.

Studies have also been reported that examine the combination of wind and solar technologies with low temperature electrolysers. The modelling has focused on controlling the power to the electrolyser with variations in power load from wind turbines as well as controlling the power output to the grid from the electrolyser/wind turbine hybrid system (Zhou and Francois, 2009). Solar photovoltaic cells were shown to produce hydrogen from electrolysers at thermal efficiencies of 10.9% (Bilgen, 2001) and around 8% (Clarke et al., 2009).

The SOEC model applied here assumes that the electrolyser operates under steady-state conditions (Hernández-Pacheco et al., 2004; Ni et al., 2006), with most of the steam reduction reaction occurring at a 2D interface between the electrode and electrolyte, rather than at distributed three phase boundaries (TPBs) within a 3D porous electrode (Chan and Xia, 2002; Ni et al., 2006). It is also assumed that the thickness of the electrodes is sufficiently small for the concentration of species to be uniform across the thickness of the electrode (Ni et al., 2006; Udagawa et al., 2008). Furthermore, temperature gradients across the electrodes have been neglected as it has been assumed that the operating temperature of the cell is constant. A sufficient pressure gradient is produced at the anode side for the O_2 produced to permeate through the anode (Ni et al., 2006). Ideal gas behaviour has been assumed for the gas streams (Udagawa et al., 2008).

The equations governing the performance of the SOEC model is composed of mass transfer, energy requirements and cell potential and a schematic is shown in Fig. 2. The thermodynamic equations calculate the enthalpy (ΔH) and Gibbs free energy (ΔG), to show the minimum amount of total energy and electrical energy, respectively, needed for the reaction (Eq. (1)). Enthalpy sets the theoretical energy requirement which is used to calculate the SOEC efficiency. Gibbs free energy is used to calculate both the Nernst (the voltage when current is zero) and the reversible (E_{rev}) potentials.

The reversible potential (E_{rev}), which is based on ΔG, together with ohmic (E_{ohm}), activation ($E_{act,tot}$), and concentration ($E_{conc,tot}$), overpotentials account for the operating potential (E_{op}). The operating potential is used to find the heat energy produced by electrolysis (Joule heating and overpotentials).

The energy analysis considers the power necessary for raising steam to the desired SOEC operating conditions and the power required for the electrolysis process. The resistances occurring during electrolysis, which are affected by temperature and pressure, generate thermal energy ($\dot{Q}_{electrolysis}$). In addition, heat is introduced to the system by the entering steam ($\dot{Q}_{steam}$). The total thermal energy ($\dot{Q}_{total}$), allows a thermal analysis to be carried out based on the varying conditions of the steam. Furthermore, a basis for optimisation can be found at the thermoneutral voltage (E_{tn}), the point at which the heat for the reaction (endothermic) is equal to the heat produced by Joule heating and electrode overpotentials. The SOEC efficiency combines the equations based on the amount of energy from the H_2 produced compared with the energy required to meet the operating conditions of the cell.

2.1. *Mass transfer*

The mass transport of components to and from the electrolyte is complex due to the porosity of the electrode material and therefore is based on diffusion at the cathode and permeation at the anode through the three phase boundaries, which refers to the regions in the porous material of the electrode where the ceramic, metal and reactants meet.

2.1.1. *Cathode*

At steady state, the mass transport of a component can be represented by (Geankoplis, 1972; Ni et al., 2006):

$$\nabla \dot{N}_i = \frac{\delta \dot{N}_i}{\delta x} + \frac{\delta \dot{N}_i}{\delta y} + \frac{\delta \dot{N}_i}{\delta z} = 0 \quad (2)$$

which represents the change in the flow of component in directions x, y and z.

Steam is supplied to the cathode via convection; however, once at the electrode surface, diffusion occurs to the active sites for reaction. Due to the complex nature of porous materials, an average effective diffusivity term is used, which takes

into account Knudsen and molecular diffusion. Knudsen diffusion takes into account gases passing through the smaller pores of the cathode and molecular diffusion accounts for mass transport through larger pores.

The concentrations at the three phase boundaries are based on Fick's law of diffusion (Geankoplis, 1972):

$$J^*_{H_2O} = -D_{Aeffave}\frac{\delta C_{H_2O}}{\delta x} \tag{3}$$

where $J^*_{H_2O}$ is the diffusion flux of H_2O flowing through the electrode in the x-direction and $D_{Aeffave}$ is the average diffusivity. Generally, a small amount of hydrogen is included in the inlet to provide a reducing environment to ensure the Ni in the cathode does not oxidise to NiO.

The molar flux, $\dot{N}_{H_2O}$, can be used to describe the diffusion and flow of components in a system based on the diffusion flux and the convective flux, which is the product of concentration, C_{H_2O}, and molar average velocity, v^* (Geankoplis, 1972):

$$\dot{N}_{H_2O} = J^*_{H_2O} + v^* C_{H_2O} \tag{4}$$

For a system such as electrolysis, where steam in the gaseous phase reacts to produce another gas, hydrogen, at constant pressure and steady state, molecular diffusion of steam occurs. Assuming that the reaction at the boundary is fast, which results in a small mole fraction and hence a small concentration of steam; the convective flux can be deemed negligible (Geankoplis, 1972). Eq. (4) can therefore be simplified to:

$$\dot{N}_{H_2O} = J^*_{H_2O} = -D_{Aeffave}\frac{\delta C_{H_2O}}{\delta x} \tag{5}$$

By substituting Eq. (5) into (2) and considering the diffusion through the electrode only occurring in the x-direction through the thickness of the electrode, i.e. $x = \tau_{cathode}$ (Ni et al., 2006):

$$\nabla \dot{N}_{H_2O} = \frac{\delta \dot{N}_{H_2O}}{\delta x} = \frac{\delta}{\delta x}\left(-D_{Aeffave}\frac{\delta C_{H_2O}}{\delta x}\right) = 0 \tag{6}$$

The flow of components to the cell can be expressed by the current density, i:

$$\dot{N}_{H_2O} = \frac{i}{nF} \tag{7}$$

Substituting Eq. (7) into (5) gives:

$$\frac{i}{nF} = -D_{Aeffave}\frac{\delta C_{H_2O}}{\delta x} \tag{8}$$

Across the electrode there are variations in the concentration of components. The fixed boundary is the thickness of the electrode and therefore, concentration profiles can only occur within this layer; the boundary condition for Eq. (6) is given by:

$$\left.\frac{\delta C_{H_2O}}{\delta x}\right|_{x=\tau_{cathode}} = -\frac{i}{nFD_{Aeffave}} \tag{9}$$

The amount of steam at the surface of the cathode can be denoted as the concentration of steam at the point where the thickness in the x-direction is zero and is as follows:

$$C_{H_2O}\big|_{x=0} = C^0_{H_2O} \tag{10}$$

Solving Eq. (6) with the boundary conditions in Eqs. (9) and (10) gives the concentration of steam at the boundaries (Udagawa et al., 2007):

$$C^{TPB}_{H_2O} = C^0_{H_2O} - \frac{i\tau_{cathode}}{nFD_{Aeffave}} \tag{11}$$

The rate of the production of hydrogen is equal to the rate of consumption of steam, which means that the pressure remains constant; and a similar equation can therefore be written for the hydrogen produced at the cathode (Udagawa et al., 2007):

$$C^{TPB}_{H_2} = C^0_{H_2} - \frac{i\tau_{cathode}}{nFD_{Aeffave}} \tag{12}$$

The average effective diffusivity, $D_{Aeffave}$ takes into account both the Knudsen diffusion for the gases through the smaller pores of the cathode as well as the molecular diffusion, which takes place when the pores are larger.

$$\frac{1}{D_{AeffH_2O}} = \frac{\xi}{\varepsilon}\left(\frac{1}{D_{H_2O-H_2}} + \frac{1}{D_{kH_2O}}\right)$$
$$\frac{1}{D_{AeffH_2}} = \frac{\xi}{\varepsilon}\left(\frac{1}{D_{H_2O-H_2}} + \frac{1}{D_{kH_2}}\right) \tag{13}$$

where $D_{H_2O-H_2}$ represents the molecular diffusion and, D_{kH_2} and D_{kH_2O} are the Knudsen diffusion for hydrogen and steam, respectively. ξ and ε represent the tortuosity and porosity, respectively.

The Knudsen diffusion for each component, D_{ki} is given by (Ni et al., 2006):

$$D_{ki} = \frac{4}{3}r_p\sqrt{\frac{8RT}{\pi MW_i}} \tag{14}$$

where MW_i is the molecular weight of each component and r_p is the pore radius.

The radius of the pore, r_p, is given by (Chan et al., 2001):

$$r_p = \frac{2\varepsilon}{S_A\rho_B} \tag{15}$$

where S_A represents the surface area of the pore and ρ_B is the bulk density.

The molecular diffusion of the gases through large pores in the electrodes is given by (Lightfoot et al., 2002):

$$D_{H_2O-H_2} = 0.0018583 \times \sqrt{T^3\left(\frac{1}{MW_{H_2O}} + \frac{1}{MW_{H_2}}\right)} \times \frac{1}{P\delta^2_{H_2O-H_2}\Omega_{DH_2O-H_2}} \tag{16}$$

where P represents the total pressure (atm), δ is the collision diameter and $\Omega_{DH_2O-H_2}$ is the collision integral.

The collision integral, $\Omega_{DH_2O-H_2}$, can be interpolated from known T^* values as shown in by Geankoplis (1972), and is a function of the Lennard–Jones potential, which includes the operating temperature and the characteristic energy for each component, ε_{ki}:

$$T^* = \frac{k_B T}{\varepsilon_{kH_2O-H_2}} \tag{17}$$

where T^* refers to the Lennard–Jones potential and k_B is the Boltzmann constant, and $\varepsilon_{kH_2O-H_2} = (\varepsilon_{kH_2O}\varepsilon_{kH_2})^{0.5}$. The collision diameter, δ_i, is given as:

$$\delta_{H_2O-H_2} = \frac{\delta_{H_2O} + \delta_{H_2}}{2} \tag{18}$$

where the average diffusivity, $D_{Aeffave}$, of the gas mixture at the three phase boundary is:

$$D_{Aeffave} = \frac{p^0_{H_2O}}{P} D_{AeffH_2O} + \frac{p^0_{H_2}}{P} D_{AeffH_2} \tag{19}$$

2.1.2. Anode

The flow of the components leaving at the anode side is assumed to be only oxygen and therefore, only permeation occurs rather than diffusion. The gas viscous flow is usually characterised through Darcy's law shown in Eq. (20) (Jeon et al., 2006):

$$\dot{N}_{O_2} = \frac{-B_g}{RT\mu} \frac{p_{O_2}}{\tau_{anode}} \nabla P_{O_2} \tag{20}$$

where B_g is the flow permeability and μ is the dynamic viscosity shown in Eqs. (21) and (22), respectively.

$$B_g = \frac{\varepsilon^3}{72\xi(1-\varepsilon)^2}(2r_p)^2 \tag{21}$$

$$\mu = \sum_{d=0}^{6} b_d (T^{**})^d \tag{22}$$

where

$$T^{**} = \frac{T(K)}{1000} \tag{23}$$

Recall Eq. (2) for oxygen:

$$\nabla \dot{N}_{O_2} = \frac{\delta \dot{N}_{O_2}}{\delta_x} + \frac{\delta \dot{N}_{O_2}}{\delta_y} + \frac{\delta \dot{N}_{O_2}}{\delta_z} = 0$$

Combining Eqs. (2) and (20), we can describe the oxygen transport in the anode as (Ni et al., 2006):

$$\frac{\delta}{\delta x}\left(-\frac{B_g p_{O_2}}{RT\mu\tau_{anode}} \frac{\delta p_{O_2}}{\delta x}\right) = 0 \tag{24}$$

At the electrolyte–electrode interface, where the oxidation reaction occurs, the rate of oxygen production can be shown in terms of the current density:

$$N_{O_2} = -\frac{i}{4F} \tag{25}$$

where the number of electrons, n, needed to form 1 mol of an oxygen molecule is 4.

The boundary conditions at the thickness of the electrode can then be represented by:

$$p_{O_2} \frac{\delta p_{O_2}}{\delta x}\bigg|_{x=\tau_{cathode}} = \frac{iRT\mu}{4FB_g} \tag{26}$$

The amount of oxygen at the surface of the anode boundary can be denoted by:

$$p_{O_2}\big|_{x=0} = p^0_{O_2} \tag{27}$$

Based on the boundary conditions in Eqs. (26) and (27), Eq. (24) can be solved to find the partial pressure of oxygen at the three phase boundaries (Ni et al., 2006):

$$p^{TPB}_{O_2} = \sqrt{(p^0_{O_2})^2 + \frac{RTi\mu\tau_{anode}}{2FB_g}} \tag{28}$$

where $p^{TPB}_{O_2}$ is the partial pressure of oxygen at the TPBs and $p^0_{O_2}$ is the partial pressure of oxygen at the inlet.

2.2. Cell potential

The potential of the cell dictates the performance of the electrolyser and takes into account the theoretical potential as well as resistances created by electrolysis. The electrochemical equations presented in this section aims to find the overpotentials and operating potentials, thus estimating the efficiency of the cell.

In reality, the system will have resistances, which produce overpotentials. The total overpotentials include that of ohmic (E_{ohm}), activation ($E_{act,tot}$) and concentration ($E_{conc,tot}$) losses. The overpotentials need to be overcome in order for the SOEC to function effectively; therefore, a larger voltage is required for the operation of an electrolyser above the Nernst potential, which is accounted for by the operating potential (E_{op}) (Udagawa et al., 2007):

$$E_{op} = E_{rev} + E_{ohm} + E_{act,tot} + E_{conc,tot} = E_{rev} + E_{overpot} \tag{29}$$

For an electrolyser where there is a potential difference, E, between two electrodes and charge transfer through the circuit, electrical work (W_{elec}) is being done on the system (Smith et al., 2005):

$$W_{elec} = qE = nFE = \Delta G \tag{30}$$

where n relates to the number of electrons per mole. For the reaction in Eq. (1), the change in the Gibbs free energy can be written as (Gupta, 2008):

$$\Delta G = \Delta G^{\circ}_0 + RT \ln\left[\frac{\alpha_{H_2}\alpha^{0.5}_{O_2}}{\alpha_{H_2O}}\right] \tag{31}$$

where ΔG°_0 is the Gibbs free energy at standard temperature and pressure of 25 °C and 1 atm, respectively and α_i is the activity of each component involved in the reaction. The activity of an ideal gas is the relationship between the partial pressure of the gas relative to standard conditions (i.e. p_i/p^0). Combining Eqs. (30) and (31), gives Eq. (32) which shows the Nernst potential or reversible potential, E_{rev}, written in terms of partial pressure (Gupta, 2008):

$$E_{rev} = E_0 + \frac{RT}{nF} \ln\left[\frac{p_{H_2} p^{0.5}_{O_2}}{p_{H_2O}}\right] \tag{32}$$

where E_0 represents the potential between the electrodes at a constant pressure and temperature at zero current, and p_i is the partial pressure of components. The reversible potential represents the open circuit voltage (OCV), which is when there is no flow of current between electrodes, at the SOEC operating temperature.

At standard conditions, the equilibrium voltage for electrolysis of the reactant is represented by E_0°:

$$E_0^\circ = -\frac{\Delta G_0^\circ}{nF}, \quad E_0 = -\frac{\Delta G}{nF} \tag{33}$$

For each one mole of steam, two electrons are required and the associated charge (q) transfer between the electrodes is shown in Eq. (34) (Smith et al., 2005):

$$q = 2N_A(-e) = 2F \tag{34}$$

where N_A is Avogadro's number, F is Faraday's constant and e is the charge on an electron.

2.2.1. Ohmic overpotential

The ohmic overpotentials, E_{ohm}, are produced as a result of the resistance to the current through the electrodes and ions through the electrolyte (Udagawa et al., 2007).

$$E_{ohm} = i\left(\frac{\tau_{cathode}}{\sigma_{cathode}} + \frac{\tau_{electrolyte}}{\sigma_{electrolyte}} + \frac{\tau_{anode}}{\sigma_{anode}}\right) \tag{35}$$

where σ_{anode}, $\sigma_{cathode}$ and $\sigma_{electrolyte}$ is the conductivity, τ_{anode}, $\tau_{cathode}$ and $\tau_{electrolyte}$ are the thickness of the anode, cathode and electrolyte, respectively and i is the current density. This model considers the resistances from the electrical connections and contacts to be negligible.

2.2.2. Activation overpotential

Activation overpotential, $E_{act,tot}$, is derived from the Butler–Volmer equation, assuming the charge transfer coefficients of the anode and cathode are equal (Chan et al., 2001; Udagawa et al., 2007; Laurencin et al., 2011; Mench, 2008).

$$E_{act,tot} = \left[\frac{RT}{F}\arcsin h\left(\frac{i}{2i_{0,anode}}\right)\right] + \left(\frac{RT}{F}\arcsin h\left(\frac{i}{2i_{0,cathode}}\right)\right) \tag{36}$$

The overpotential is related to the charge transfer process and kinetics of the reaction at each electrode–electrolyte interface and accounts for the energy required to overcome the activation energy constraint of the reaction (Chan et al., 2001; Mench, 2008). The activation energy needs to be overcome both thermally and electrically (Zhu and Kee, 2003). The activation overpotential is also a function of the exchange current densities, $i_{0,cathode}$ and $i_{0,anode}$ which represents the catalytic behaviour of the electrode to determine the rate of oxidation or reduction of the reaction.

2.2.3. Concentration overpotential

Concentration (mass transport) overpotentials are formed at times when there is resistance to the flow of reactant to, and product away from, the three phase boundaries, which are the regions in the porous material where the ceramic, metal and reactants meet and which is where the steam reduction reaction occurs. The total concentration overpotential takes into account the concentration overpotentials occurring on both electrodes of the SOEC and is given by:

$$E_{conc,tot} = E_{conc,anode} + E_{conc,cathode} \tag{37}$$

The concentration overpotential, $E_{conc,cathode}$, at the cathode is given by (Cai et al., 2012):

$$E_{conc,cathode} = \frac{RT}{2F}\ln\left[\left(\frac{C_{H_2}^{TPB}C_{H_2O}^{0}}{C_{H_2O}^{TPB}C_{H_2}^{0}}\right)\right] \tag{38}$$

where $C_{H_2O}^0$, $C_{H_2}^0$, $C_{H_2O}^{TPB}$ and $C_{H_2}^{TPB}$ are the concentrations of steam and hydrogen at the surface of the electrode and at the three phase boundaries, respectively. The concentration overpotential at the anode side assumes that only O_2 is present and thus permeation takes place through the electrode (Ni et al., 2006):

$$E_{conc,anode} = \frac{RT}{4F}\ln\left(\frac{p_{O_2}^{TPB}}{p_{O_2}^{0}}\right) \tag{39}$$

where $p_{O_2}^0$ and $p_{O_2}^{TPB}$ are the partial pressures of oxygen at the surface of the electrode and at the TPBs, respectively.

2.3. Energy requirement

2.3.1. Thermodynamic

The thermodynamic equations represent the total minimum energy requirements for the electrolysis reaction (Eq. (1)), which is comprised of the sum of the electrical (ΔG) and thermal (Q) energies needed for the reaction to occur. $T\Delta S$ is equivalent to the heat energy of the system at a certain temperature and pressure, with no changes in the system the available heat in the system is constant. At a stable temperature and pressure, the enthalpy remains constant and so does the available heat, which thereby identifies the amount of electrical energy required to meet the minimum energy needed for the reaction.

The total minimum energy required for the reaction is governed by the enthalpy, ΔH (Smith et al., 2005):

$$\Delta H = \Delta G + T\Delta S = \Delta G + Q \tag{40}$$

where T is the operating temperature and ΔS is the entropy change of the system. The Gibbs free energy, ΔG, represents the amount of energy available within the system at constant temperature and pressure and governs whether the reaction will take place (Smith et al., 2005):

$$\Delta G = \Delta H_0^\circ - \frac{T}{T_0}(\Delta H_0^\circ - \Delta G_0^\circ) + R\int_{T_0}^{T}\frac{\Delta C_p^\circ}{R}dT - RT\int_{T_0}^{T}\frac{\Delta C_p^\circ}{R}\frac{dT}{T} \tag{41}$$

Enthalpy can also be written in the following form:

$$\Delta H = \Delta H_0^o + R\int_{T_0}^{T}\frac{\Delta C_p^o}{R}dT \tag{42}$$

where ΔH_0° is the enthalpy at standard temperature of 25 °C and R is the universal gas constant.

For each component in the reaction, υ_i is the stoichiometric coefficient and A_i, B_i, C_i and D_i are heat capacity constants.

$$\Delta A = \sum_i \upsilon_i A_i \quad \Delta B = \sum_i \upsilon_i B_i \quad \Delta C = \sum_i \upsilon_i C_i \quad \Delta D = \sum_i \upsilon_i D_i \tag{43}$$

The reduced temperature, t, is defined as:

$$t \equiv \frac{T}{T_0} \tag{44}$$

The enthalpy is dependent on temperature and the components involved, which are related to the specific heat capacity of the components, ΔC_p° (Smith et al., 2005):

$$\int_{T_0}^{T} \frac{\Delta C_p^\circ}{R} dT = (\Delta A)T_0(t-1) + \frac{\Delta B}{2}T_0^2(t^2-1) + \frac{\Delta C}{3}T_0^3(t^3-1) + \frac{\Delta D}{T_0}\left(\frac{t-1}{t}\right) \tag{45}$$

Eq. (46) is the second integral of Eq. (45) and is based on the second law of thermodynamics.

$$\int_{T_0}^{T} \frac{\Delta C_p^\circ}{R}\frac{dT}{T} = \Delta A \ln t + \left[\Delta B T_0 + \left(\Delta C T_0^2 + \frac{\Delta D}{t^2 T_0^2}\right)\left(\frac{t+1}{2}\right)\right](t-1) \tag{46}$$

2.3.2. *Additional energy requirement*

In addition to the thermodynamic requirements, energy is also necessary to overcome overpotentials and for heating and cooling the cell in order to maintain its operating conditions. It is important to identify the thermoneutral point at which the heat produced by the overpotentials is equal to the heat required for the reaction. Current densities above this point would require cooling of the system as the overpotentials dominate, and current densities below this point would require heating to service the endothermic reaction. The extent of heating or cooling required must therefore be considered.

Fig. 1 illustrates the power needed for providing the heat associated with the process. $\dot{Q}_{steam}$ considers the power needed to raise the feed to the operating temperature and pressure of the system:

$$\dot{Q}_{steam} = \dot{m}_{H_2O} C_p (T - T_{feed}) \tag{47}$$

where $\dot{m}_{H_2O}$ is the mass flow rate of steam and T_{feed} is the temperature of the feed inlet. The total power required for electrolysis, $\dot{Q}_{electrolysis}$, is the sum of the energy generated by the overpotentials, $\dot{Q}_{overpotential}$, and the heat needed for the endothermic steam electrolysis reaction, $\dot{Q}_{reaction}$:

$$\dot{Q}_{electrolysis} = i\left(-E_{op} + \frac{\Delta H}{nF}\right) \tag{48}$$

As shown in Eq. (29), the overpotentials are an integral part of the operating potential and therefore $\dot{Q}_{overpotential}$ is represented by iE_{op} in Eq. (48). $\dot{Q}_{reaction}$ is represented by $i\Delta H/nF$ of Eq. (48) and shows the minimum amount of power required to enable the progression of the steam reduction reaction based on the enthalpy, ΔH, calculated in the thermodynamic model (Eq. (42)).

Finding a balance between driving the reaction and maintaining the operating conditions is essential. The total amount of thermal power required for electrolysis based on the energy from the steam inlet and the heat from the overpotentials is given by:

$$\dot{Q}_{total} = \dot{Q}_{electrolysis} + \dot{Q}_{steam} \tag{49}$$

Table 1 – Values taken from literature to validate the model.

Overpotential	Values from literature	
Ohmic (Udagawa et al., 2007)	$\tau_{cathode}$ (m)	500×10^{-6}
	τ_{anode} (m)	50×10^{-6}
	$\tau_{electrolyte}$ (m)	20×10^{-6}
	$\sigma_{cathode}$ (Ω^{-1} m^{-1})	8×10^4
	σ_{anode} (Ω^{-1} m^{-1})	8.4×10^3
	$\sigma_{electrolyte}$ (Ω^{-1} m^{-1})	1.416
	T (°C)	750
Activation (Chan and Xia, 2002)	$i_{0,cathode}$ (A m^{-2})	5300
	$i_{0,anode}$ (A m^{-2})	2000
	T (°C)	800
Concentration: cathode (Udagawa et al., 2007)	$\tau_{cathode}$ (m)	500×10^{-6}
	C_{H_2O} (mol m^{-3})	10.58
	C_{H_2} (mol m^{-3})	1.17
	D_{eff} (m^2 s^{-1})	1.416
	T (°C)	750
	P (atm)	1
Concentration: anode (Ni et al., 2006)	τ_{anode} (m)	500×10^{-6}
	B_g (m^2)	1.28×10^{-16}
	r_m (m)	5×10^{-7}
	μ (Pa s)	5.13×10^{-5}
	ξ	6
	ε	0.3
	T (°C)	800
	P_{inO_2} (atm)	0.2

2.4. *Efficiency*

The energy efficiency of the SOEC is given by:

$$Efficiency = \frac{2F(E_{op} - E_{overpot})\dot{N}_{H_2}}{(iE_{op}) + \dot{Q}_{steam}} \times 100 \tag{50}$$

The efficiency takes into consideration the theoretical voltage required for electrolysis ($E_{op} - E_{overpot}$) compared with the total power input to the system ($iE_{op} + \dot{Q}_{steam}$), which is related to the amount of hydrogen produced. The theoretical power required is calculated from the operating potential used to operate the SOEC and the overpotentials (resistances produced by the movement of species and reaction). The total energy required to operate the cells is accounted for by considering the power input for electrolysis as well as the additional power consumed for conditioning the inlet steam.

3. SOEC model implementation and results

The model was validated against literature values shown in Table 1 and showed excellent correlations with published work, with errors of within 2% (Chan et al., 2001; Ni et al., 2006; Udagawa et al., 2007).

One of the greatest challenges related to SOECs is improving the efficiency in order for the cost and quantity of producing H_2 to become competitive with SMR. The largest operating cost has been shown to be the electricity required for electrolysis, and improving SOEC efficiency would therefore enable the cost of producing H_2 to decrease (Manage et al., 2011). In addition, some studies have highlighted that

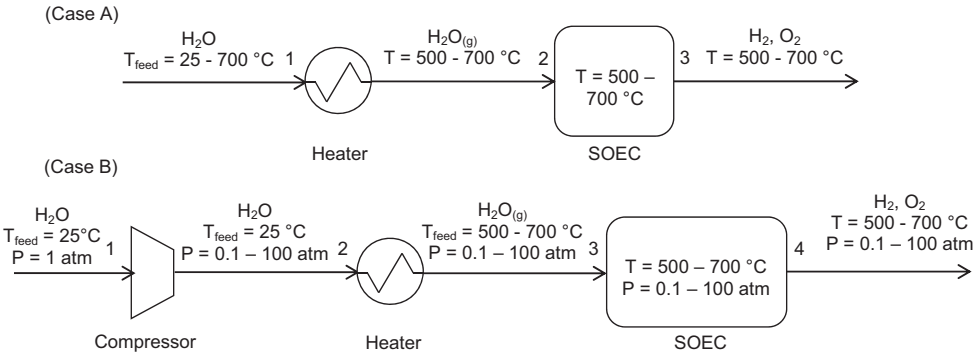

Fig. 3 – Process flow diagrams showing modelled systems: Case A – the entering feed is heated and then used to operate the SOEC. Case B – the entering feed is pressurised, heated and used to operate the SOEC.

pressurised systems improve efficiency, especially as pressurising water prior to use requires less energy than pressuring hydrogen after the electrolysis process (O'Brien et al., 2010; Roy et al., 2006; Santarelli et al., 2009). However, raising the pressure of water initially requires more energy than at atmospheric pressure and therefore a trade-off is required (O'Brien et al., 2010).

One of the greatest impacts on the efficiency of H_2 production from SOECs is the energy required to raise the steam to the required operating temperature, and potentially pressurise the system as well. Making use of high-grade steam is one option for improving the overall efficiency of the system.

In order to move SOEC technology towards commercialisation, the efficiencies seen on lab scale systems need to be maintained through scale-up. Steam for electrolysis is commonly produced from a reservoir of water and heated to the temperatures required for the SOECs (Stoots et al., 2010; Mougin et al., 2012). Efficiency and cost have been noted as barriers to commercialisation, and therefore to improve efficiency, heating water to operating conditions using hot streams from nuclear plants and solar energy has been studied (Shin et al., 2007; Fujiwara et al., 2008; Bo et al., 2010; Zhang et al., 2013). The extent of the improvement in SOEC efficiency by using hot streams from sources such as coal fired power plants and other suitable chemical plants, rather than raising steam from water will be assessed in the following.

In the following, we have considered integrating an existing power plant with an SOEC system. Case A assumes that inlet water or steam (stream 1 in Figs. 1 and 3) for the SOEC could be sourced from a number of locations in the power plant at temperatures ranging between 25 and 700 °C at 1 atm, as shown in Fig. 3 (Case A). In order for the feed stream to be suitable for use in the SOECs at an assigned operating temperature, the inlet stream would have to be either heated or cooled. It has been assumed that the heater is operated at 100% efficiency. The effect on the overall efficiency of the SOEC, based on the amount of energy required for producing suitable steam, has been the main objective of our study.

Though there are advantages to using pressurised steam for electrolyser operation, such as a reduction in area specific resistance and the ability to carry a larger flow rate, the energy consumption for both pressurising and heating the steam prior to the SOEC may outweigh the benefits achieved from sourcing steam already at suitable conditions (O'Brien et al., 2010). General Case B considers the energy consumption of producing hot and pressurised steam from water sourced at 25 °C and 1 atm. The power requirements for both these two cases are calculated to investigate the effect on the efficiency of the cell. The parameters used for the general case is shown in Table 2.

This study is focused on intermediate temperature SOEC operation, which generally refers to temperatures of between 500 and 700 °C (Baek et al., 2012; Huang et al., 2012). Intermediate temperature operation, rather than high temperature operation, offers advantages such as shorter start-up times and durability as well as allowing a range of more cost-effective materials to be used (Zhen et al., 2008; Huang et al., 2012). As such, conventionally used intermediate temperature materials have been chosen; gadolinium doped cerium oxide (CGO) electrolyte, lanthanum strontium cobalt ferrite (LSCF) anode and Ni–CGO cermet cathodes in a planar configuration. Ni–CGO and CGO have shown good conductivities in SOFCs (Zhen et al., 2008; Choi et al., 2013). The parameters that have the most significant impact on the model are the conductivity and exchange current densities with the latter varying in orders of magnitude with changing temperatures. The majority of experimental studies have investigated electrolysis using YSZ electrolytes and more recently, detailed studies on the properties of the material have been tested (Aruna et al., 1998; Shin et al., 2007; Kim-Lohsoontorn and Bae, 2011b; Manage et al., 2011).

Although ceria has been studied in fuel cell mode (Livermore et al., 2000; Veranitisagul et al., 2012; Liu et al., 2013), data available for the characteristics of CGO and Ni–CGO as electrolyser material is limited (Pérez-Coll et al., 2003; Muecke et al., 2008; Othman et al., 2010). Therefore, to provide a realistic representation of the changes in material performance with temperature, it has been assumed that Ni–CGO, the chosen material for this study, has a similar behaviour to Ni–YSZ as Ni–CGO is also a ceramic metal mixture (cermet) like Ni–YSZ, which has been widely researched (Matsushima et al., 1998; Marinsek et al., 2007; Kakade et al., 2011; Pihlatie et al., 2012). In particular, it has been assumed that the conductivity for Ni–CGO follows the same trend as Ni–YSZ (Steele and Heinzel, 2001; Jasinski et al., 2004). From the data on conductivity in literature for Ni–YSZ by Aruna et al. (1998), a polynomial fit was made. A known value of $6 \times 10^4\ \Omega^{-1}\,m^{-1}$ at 650 °C for Ni–CGO (Muecke et al., 2008) was used as a basis to from which to extrapolate.

A similar analysis for estimating the changes to the exchange current density with varying temperature was also carried out. It has been assumed that the exchange current density for Ni–CGO follows the same trend as that for Ni–YSZ. A correlation in literature, based on an experimental study for Ni–YSZ by Leonide et al. (2009), was fitted to an exponential equation, which is in the format of the Arrhenius equation

Table 2 – List of parameters used in the SOEC model.

Parameters	Parameter value	References
A (H_2O, H_2, O_2)	3.470, 3.249, 3.639	Smith et al. (2005)
B (H_2O, H_2, O_2)	0.001450, 0.000422, 0.000506	Smith et al. (2005)
C (H_2O, H_2, O_2)	0, 0, 0	Smith et al. (2005)
D (H_2O, H_2, O_2)	12,100, 8300, −22,700	Smith et al. (2005)
ν (H_2O, H_2, O_2)	−1, 1, 0.5	
ΔH_0°	−241.818 (kJ mol^{-1})	Smith et al. (2005)
ΔG_0°	−228.572 (kJ mol^{-1})	Smith et al. (2005)
T	773, 873, 923, 973 (K)	
T_0	273 (K)	Smith et al. (2005)
N	2	
F	96,487 (C mol^{-1})	
R	8.314 (J mol^{-1} K^{-1})	
τ_{anode}	30×10^{-6} (m)	Herring (2006)
$\tau_{cathode}$	30×10^{-6} (m)	Herring (2006)
$\tau_{electrolyte}$	100×10^{-6} (m)	Herring (2006)
x_{H_2O}	0.9	
x_{H_2}	0.1	
x_{O_2}	1	
P	1 (atm)	
M_{H_2O}	18 (g mol^{-1})	
M_{H_2}	2 (g mol^{-1})	
E	0.3	Chan et al. (2001)
S_A	6×10^4 (cm^2 g^{-1})	
ρ_B	7.119 (g cm^{-3})	
Ξ	6	Chan et al. (2001)
ε_k/k_{H_2O}	809.1 (K)	Lightfoot et al. (2002)
ε_k/k_{H_2}	59.7 (K)	Lightfoot et al. (2002)
δ_{H_2O}	2.641 (Å)	Lightfoot et al. (2002)
δ_{H_2}	2.827 (Å)	Lightfoot et al. (2002)
$\Omega_{DH_2O\text{-}H_2}$	0.87	Geankoplis (1972)
$\sigma_{cathode\ (Ni\text{–}CGO)}$ (500, 600, 650, 700 °C)	69,821, 62,575, 60,000[a], 57,902 (Ω^{-1} m^{-2})	[a]Muecke et al. (2008)
$\sigma_{0,anode\ (LSCF)}$ (500, 600, 650, 700 °C)	25,000, 28,000, 30,000, 31,000 (Ω^{-1} m^{-2})	Petric et al. (2000)
$\sigma_{electrolyte\ (CGO)}$ (500, 600, 650, 700 °C)	1.00, 3.16, 3.98, 10.0 (Ω^{-1} m^{-2})	
$i_{0,cathode\ (Ni\text{–}CGO)}$ (500, 600, 650, 700 °C)	92.9, 685.7, 1580.0[b], 3356.5 (A m^{-2})	[b]Offer and Brandon (2009)
$i_{0,anode\ (LSCF)}$ (500, 600, 650, 700 °C)	10.0[c], 130.0[c], 1800.0[d], 3328.8[d] (A m^{-2})	[c]Liu et al. (2006)[d]Zhou et al. (2010)

used for the activation overpotentials. The data used to estimate the exchange current density of Ni–CGO were then fitted to a similar function. The fit was used to extrapolate from a known value of 1580 A m^{-2} at 650 °C for Ni–CGO (Offer and Brandon, 2009).

Values from literature have been used in the model for the exchange current densities and conductivities of LSCF at varying temperatures (Petric et al., 2000), and all the parameters used in the model are shown in Table 2.

3.1. *Case A: producing hot steam at 1 atm*

The results presented are based on a general Case A whereby water/steam is fed to the system at varying temperatures between 25 and 700 °C at 1 atm, as shown in Fig. 3 (Case A). The first stage is heating the water or steam to the operating conditions. Fig. 4 shows the energy required to raise steam to 500, 600 and 700 °C, respectively, which represents the possible range of operation for CGO electrolytes (Brett et al., 2008). Using a feed stream close to the operating temperature of the SOEC, and particularly above the phase transition to steam, is clearly energetically beneficial.

The energy required to raise the temperature of the feed steam, combined with the energy necessary to operate the electrolyser, determines the overall efficiency of the system. Fig. 5 represents the change in the efficiency of the electrolyser with varying inlet feed stream temperature at a constant current density of 5000 A m^{-2}. It can be seen that as the feed temperature tends towards the operating temperature, the efficiency increases. A maximum efficiency of 71.5% was seen when the temperature of steam was raised to the operating temperature of 650 °C.

Fig. 6 represents the performance of the SOEC as the current density and feed temperatures vary. The efficiency is seen to increase with decreasing current density, as the electrical input is reduced. For example, raising the steam from 25 °C to SOEC operating conditions of 650 °C and 5000 A m^{-2}, results in system efficiency of 57%; however, raising steam from 500 °C for the same SOEC operating conditions shows an efficiency

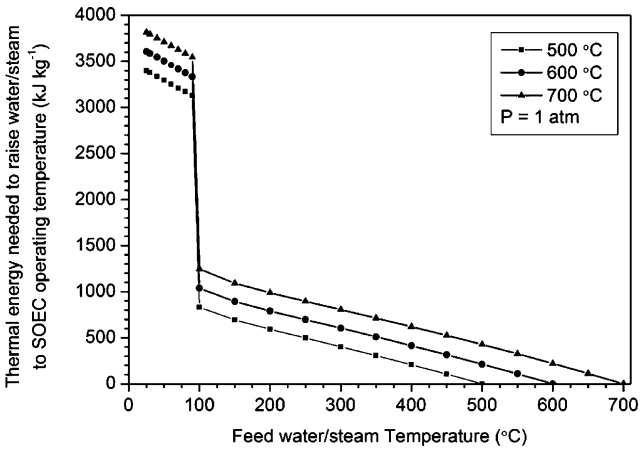

Fig. 4 – Energy required to heat water or steam to the SOEC operating temperature (500, 600 or 700 °C) at 1 atm.

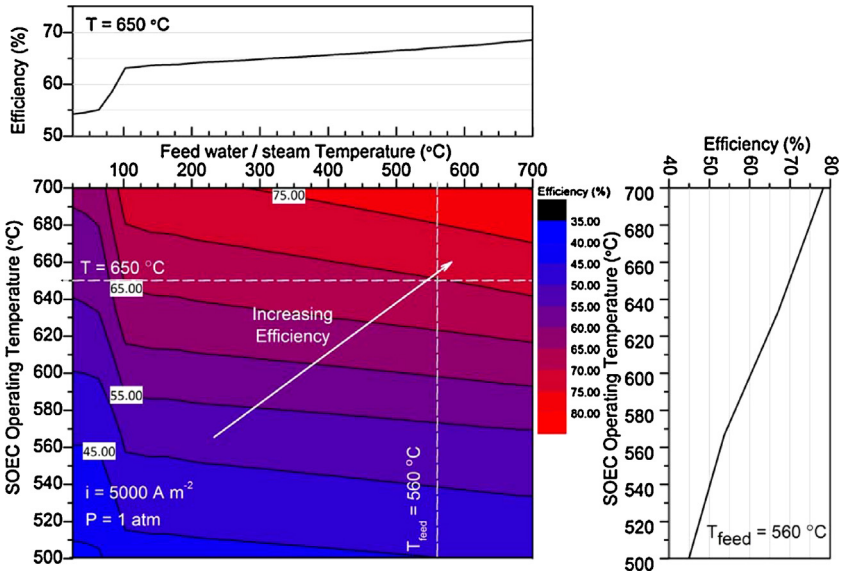

Fig. 5 – The efficiency across a range of operating temperatures and inlet feed water/steam temperatures for an SOEC operating at 5000 A m^{-2}.

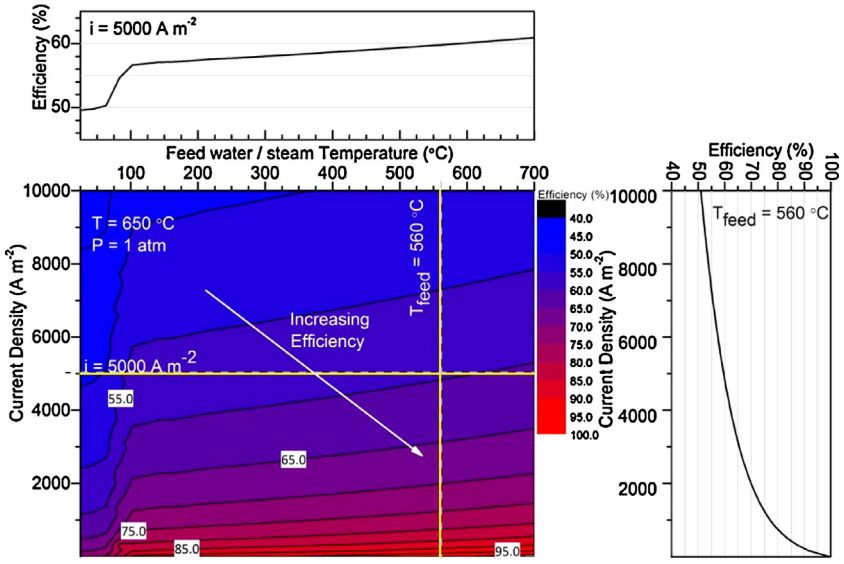

Fig. 6 – The efficiency across a range of current density and inlet feed water/steam for an SOEC operating at 650 °C and 1 atm.

of 70%. This percentage efficiency is significant and further indicates the need to source steam at suitable temperatures, if at all possible. Improvements in efficiency and reduction in energy requirement suggest a more cost effective process.

Based on these results, and in order to increase efficiency through reducing the electrical energy put into the system, a source for steam at elevated temperatures close to the SOEC operating temperature is required.

3.2. *Case B: producing hot and pressurised steam*

The results based on assessing the system described in Fig. 3 (Case B), where the inlet stream is both pressurised and heated to the SOEC operating temperature from 25 °C and 1 atm prior to entering the SOEC, are presented. The amount of thermal energy required for this process is shown in Fig. 7.

Comparing Figs. 4 and 7, it can be seen that less energy is required to raise the temperature of water as the pressure of the water increases. However, the improvement to SOEC performance and efficiency of a pressurised system is very

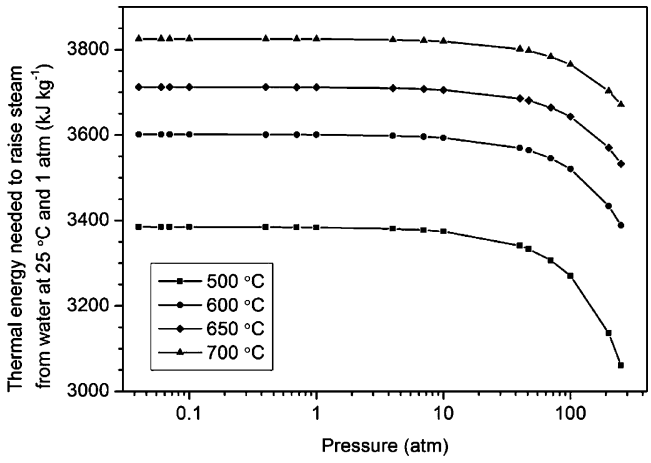

Fig. 7 – Thermal energy required for raising steam to various operating pressures at 500, 600, 650 and 700 °C from water at 25 °C and 1 atm.

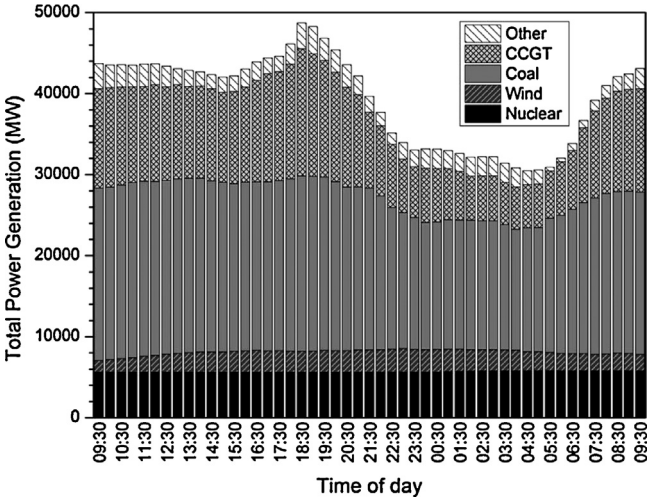

Fig. 8 – Power generation in the UK by different technologies per settlement period from 09:30 on 19.03.2012 to 09:30 on 20.03.2012. Adapted from BM reports (2012).

small. Due to this, the efficiency of the SOEC operation is very similar to that shown in Figs. 5 and 6.

Furthermore, it has been shown by Jensen et al. (2010) that an increase in pressure can reduce the overpotentials. Therefore, sourcing steam that has both elevated temperatures and pressures can provide improvement in the efficiency of the cell. The results have shown that efficiencies of around 60% can be achieved based on heating and pressurising the inlet to the SOEC, however, if streams can be sourced that are already at suitable conditions, both the performance and cost efficiency may be improved.

4. Coal fired power plants

As with many nations, the UK's energy mix includes power production through gas, coal and nuclear sources, with increasing amounts of renewable power (BM reports, 2012; Post-2020 Energy scenarios and pathways to 2030, 2012). Though there is a move towards a low carbon economy by 2050 in the UK (The Carbon Plan: Delivering our low carbon future, 2011), which is stimulated by the Climate Change Act, 2008 (The Carbon Plan: Delivering our low carbon future, 2011), the reliance on hydrocarbon-based fuels such as coal, which currently contributes to 29% of annual energy production, has been predicted to increase globally (International Energy Outlook, 2011). Therefore, it is very likely that conventional technologies such as coal fired power plants will still be operational in the near to medium future. Projections from 2008 to 2035 indicate that the use of coal in the US and UK will remain generally constant. However, a marked rise in coal use is predicted internationally, especially in countries such as China and India (International Energy Outlook, 2011).

In the UK, coal, combined cycle gas turbine, nuclear, wind, hydro, pumped storage together with French, Irish and Dutch interconnects, are regularly used for producing electricity. Though there are a number of new technologies being used in the current configuration, it can be seen from Fig. 8 that the largest power output in a 24 h period is from coal fired plants (BM reports, 2012). It also shows that technologies such as nuclear, which are not dispatchable, produce power constantly throughout the day. However, others such as coal, which are more dispatchable, are called on in times of higher power demand. During times of low demand, the power station is operated at its minimum base load, normally from 22:00 until 06:00 the next day.

Table 3 – Parameters used in the modelling of the coal fired power station.

Proximate analysis (wt%)	
Volatile material	30 min (dry basis)
Total moisture	10 max.
Specific energy	18 MJ kg^{-1} min
Ultimate analysis (wt%)	
Carbon	73.93
Hydrogen	4.65
Nitrogen	1.50
Sulphur	1.08
Oxygen	5.85
Ash	13.01
Higher heating value (HHV)	30.68 MJ kg^{-1}

Consequently, it can be assumed that hydrocarbon-based fuels, especially coal, will continue to be used in the foreseeable future. Furthermore, the cost of coal has been seen to be more attractive than gas or oil, which has resulted in plans for the construction of coal fired plants around the world with a significant growth of construction in China (EIA Country Analysis Briefs, China, 2009; Sanpasertparnich et al., 2010).

A conventional coal-fired power plant operates by combusting coal, which heats water into superheated steam. The superheated steam drives the steam cycle, also known as the Rankine cycle, where the high pressure turbine (HP), intermediate pressure turbine (IP) and low pressure turbine (LP) are driven, which in turn rotates the shaft for power generation (Drbal et al., 2005; Woodruff et al., 2005).

Supercritical power stations operate with steam above the supercritical temperature and pressure, 374.15 °C and 218 atm, most of which are used in Europe due to increased efficiencies compared with subcritical plants. In general, efficiencies vary between 36.7–38.6% and 39.2–41.3% for subcritical and supercritical plants, respectively (Beér, 2007; Yeh and Rubin, 2007).

As power plants are cyclical in the way that they are operated, i.e. turndown (but not shut down) in the night, and turn-up during times of peak energy demand; they are a possible option for integrating with SOECs, as both electricity and steam can be sourced from the plant. In order to assess the conditions of each stream of the plant and whether they are suitable for SOECs, a power station model has been developed.

A steady-state simulation of a simplified conventional 350 MW_e supercritical coal fired power plant was developed in CHEMCAD 6.0 (Chemstations^{TM}, 2008) using data in Table 3. The conditions for the superheater are 250 atm at 560 °C and reheat conditions of 46 atm at 560 °C with LP operation at 0.05 atm. The exit temperature of the flue gas under standard operation is 340 °C (Market-Based advanced coal power systems, 1999; Paiton III Power Station, 2009). The results from the simulation aim to show the operating conditions of the plant and the extent of the reduction in efficiency as the plant is turned down through steam extraction. The simulations were run with the power plant operating at full capacity, i.e. the coal and make up water input remained constant. A schematic of the plant is shown in Fig. 9.

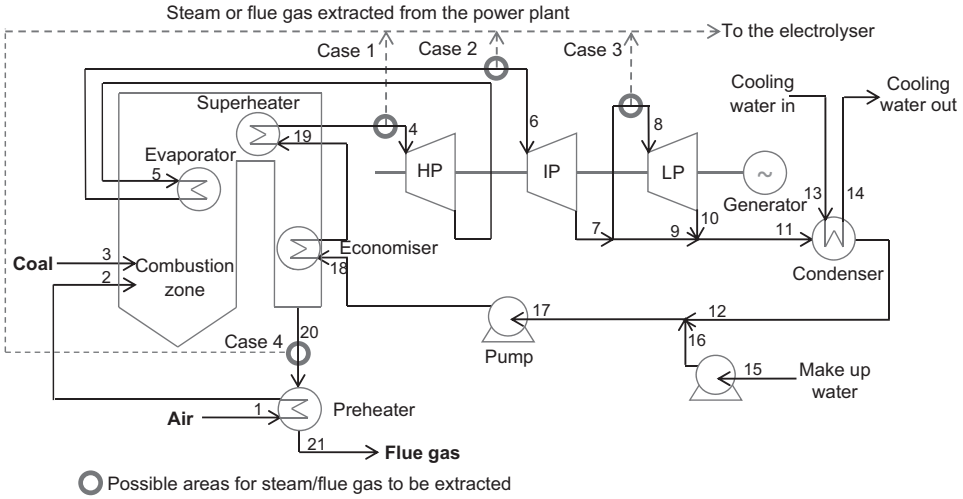

Fig. 9 – A flow sheet to represent the coupling of streams from the power plant with the SOEC. The diagram refers to Cases 1, 2 and 3 from the power plant.

5. Power plant simulation results

One of the aims of this work was to gain an understanding of the options available for extracting steam and the conditions of said streams, as well as to further examine the extent of turndown via steam removal on the plant's operation, rather than a reduced load.

Possible streams from the plant, which can provide high temperature and pressurised steam, were seen to be before the HP, IP and LP turbines, which have been assigned as Cases 1, 2 and 3, respectively. Utilising flue gas is also an option (Case 4). It should be noted that extraction from the turbines itself is possible; however, it is not considered in this study for simulation simplification (Chalmers et al., 2009; Sanpasertparnich et al., 2010). The available steam extraction points are shown in the dashed lines in Fig. 9.

In order to assess the feasible amount of steam extraction, whilst the plant's operating requirements are met, the maximum 50% turndown was used as a basis (Drbal et al., 2005). Based on this, it can be seen in Table 4 that a maximum possible amount of steam removed from the plant for Cases 1, 2 and 3 are 27%, 35% and 40%, respectively. Based on the results from the extraction of steam, it is shown that high temperatures and pressures can be obtained. A temperature range of 409–560 °C can be obtained from the plant at pressures of up to 250 atm. The extraction of streams at each point had an effect on the plant's efficiency as shown in Fig. 10. It can be seen that the largest impact on the plant is Case 1, as the main steam, which has the capacity to do the most work, is removed. When the extracted steam or flue gas is used as reactants in SOECs, hydrogen and syngas can be produced respectively.

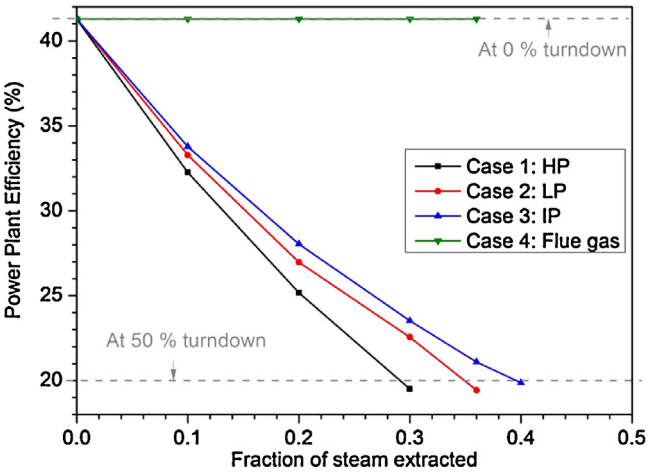

Fig. 10 – The extent of efficiency loss of the power plant with varying fractions of steam extracted for Cases 1–4.

6. System integration

In this context, system integration refers to combining an SOEC with a coal fired power plant to make the most of older technologies via retrofit, or for new systems, delivering electrical power and hydrogen fuel.

6.1. *Results of system integration*

In the following, the conditions of the steam from the power plant (Cases 1, 2 and 3) from Fig. 9 are considered to be integrated into the SOEC. It can be seen that the outlet temperature of the power station are in the range of intermediate

Table 4 – Results obtained from CHEMCAD simulations of steam extraction for Cases 1–3 for full and 50% load.

	100% load			50% load		
	Case 1	Case 2	Case 3	Case 1	Case 2	Case 3
Power plant efficiency (%)		41			20	
Steam extraction (%)		0		27	35	40
Temperature (°C)	560	560	409	560	560	409
Pressure (atm)	250	46	12.9	250	46	12.9
Flue gas exit temperature (°C)	276	276	276	785	660	681
Flow rate extracted (kg h^{-1})	0	0	0	339,000	339,000	260,000

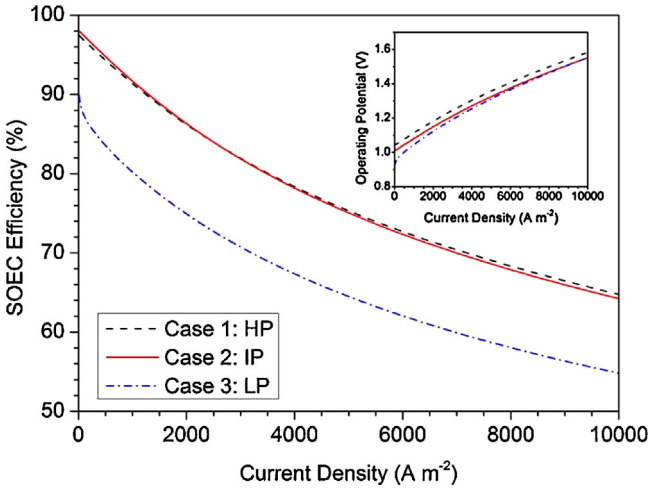

Fig. 11 – SOEC efficiency with changing current density at an operating temperature of 650 °C. The inset shows the operating potential with current density.

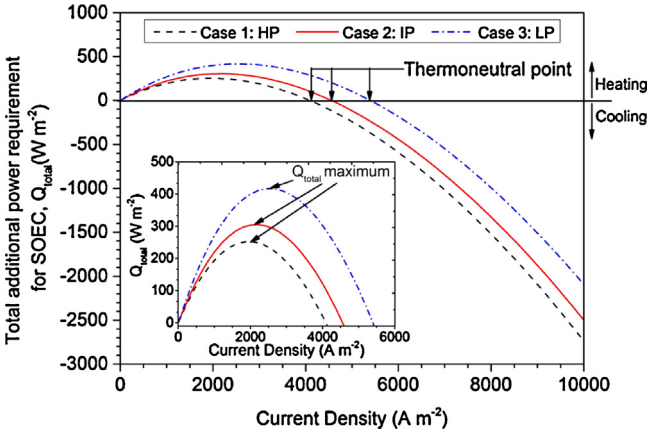

Fig. 12 – Total additional power requirement for SOEC operating at 650 °C with steam from Cases 1, 2 and 3. Inset: a close up of the peaks of the curves to show the maximum amount of additional heating power needed.

temperature operation, with a nominal SOEC temperature of 650 °C chosen for the analysis to match CGO electrolyte operating conditions (Brett et al., 2008; Offer and Brandon, 2009). The operating pressure of the SOEC system is taken to be equal to that of the feed steam extracted from the power plant. Case 4, which considers using flue gas for co-electrolysis, has not been considered in this study due to the low temperatures of the stream after particulate removal.

Fig. 11 illustrates the variations in efficiency of using steam from Cases 1 to 3 in SOECs and is based on Eq. (50). As with the general Case A (Fig. 6), the efficiency of the SOEC decreases with increasing current density and reduced inlet steam temperatures. As an example, the general Case A showed an efficiency of 60.0% when water at 25 °C was raised to 560 °C; however, an improvement to 75.3% and 75.1% at 5000 A m^{-2} was seen with the integrated system of Cases 1 and 2, respectively (results shown in Table 5). The elevated temperatures provided by the power plant means that additional energy is not needed to produce steam only to heat steam to the SOEC operating conditions, thus improving efficiency. The effect of pressure can be considered negigible as it has been shown by Jensen et al. (2010) that it has very little effect on the performance of the electrolyser.

As the steam from the power plant under certain conditions is insufficient to meet SOEC operating conditions, additional energy (taken as being in the form of electricity from the plant) to heat the steam is needed, as shown in Fig. 12. Below the zero power line, cooling is required; and the point at which the system has reached thermal equilibrium is called the thermoneutral point (at the zero power line). This is when the heat consumed by the endothermic reaction and heating steam to SOEC operating conditions is equal to that produced. The thermoneutral point expressed in this study is that of the overall system rather than just the SOEC itself. Based on the results in Fig. 12, the thermoneutral point lies at a current density of 4093, 4553 and 5296 A m^{-2} at 1.31 V for Cases 1, 2 and 3, respectively.

It should be noted that operating above the thermoneutral point may be beneficial when considering the system as a whole, as operating at current densities higher than the thermoneutral point will allow options for thermal integration. This may alleviate some of the resources extracted from the power plant, thus ensuring the overall efficiency loss is kept to a minimum.

The maximum amount of power required is 252.6 W m^{-2} (at 2000 A m^{-2}), 305.3 W m^{-2} (at 2200 A m^{-2}) and 424.3 W m^{-2} (at 2400 A m^{-2}) for Cases 1, 2 and 3, respectively. This provides the upper limit of electricity that the SOEC needs from the plant on a per metre square cell basis, as well as accounting for the further loss in power plant efficiency after steam extraction.

The extent of loss of power plant efficiency from extracting the necessary steam and electricity to operate an SOEC is shown in Fig. 13. It was seen that operating SOECs at 80% utilisation and 5000 A m^{-2} produces efficiencies of 75.3%, 75.1% and 64.5% for Cases 1, 2 and 3, respectively, which correlate with power output of hydrogen of 6.21 kW m^{-2} (0.19 kg h^{-1}) based on the lower heating value of hydrogen. The results align well with experimental data in literature, where Herring (2006) produced 3.38 kW m^{-2} (0.12 kg h^{-1}) hydrogen at 2710 A m^{-2}. (Note that the effect of both steam and electricity extraction are affected by the size of the electrolyser and the study therefore represents efficiencies based on a per metre square active area of the SOEC.)

The loss in the power plant efficiency increases non-linearly as the current density increases, due to variations in the demand of energy for heating the steam before the thermoneutral point (Fig. 13). However, after the thermoneutral point, heat is being produced, which reduces the additional energy requirements. Once the energy requirement for electrolysis and heating the steam to SOEC operating conditions have been met, additional energy is not required; only electricity to operate the SOEC.

It can be seen that operating at lower current densities gives larger SOEC efficiencies; however, the amount of hydrogen produced is also lower. Operating the SOEC higher than the thermoneutral point, such as 6000 A m^{-2}, enables larger amounts of hydrogen to be produced; however, it also has larger plant efficiency losses, with the greatest impact being Cases 1 and 3 (Fig. 13).

Overall, it can be seen from Table 5 that using the high quality heat and steam from a power plant can improve the efficiency of the electrolyser significantly, by 25% for Cases 1 and 2 and 11% for Case 3, compared with conventional methods where water is heated from 25 °C. The change in efficiency of the SOEC is almost solely dependent on the temperature of the feed rather than the pressure.

Table 5 – A comparison of SOEC efficiency based on the general and integrated cases at current densities of 5000 A m^{-2}.

General case		Integrated case		Overall improvement in SOEC efficiency (%)
Steam condition from raising water at 25 °C and 1 atm	SOEC efficiency (%) (5000 A m^{-2}, 650 °C)	Steam condition from power plant	SOEC efficiency (%) (5000 A m^{-2}, 650 °C)	
560 °C, 1 atm	60.0	560 °C, 250 atm	75.3	25.5
		560 °C, 46 atm	75.1	25.2
409 °C, 1 atm	58.0	409 °C, 12.9 atm	64.5	11.2

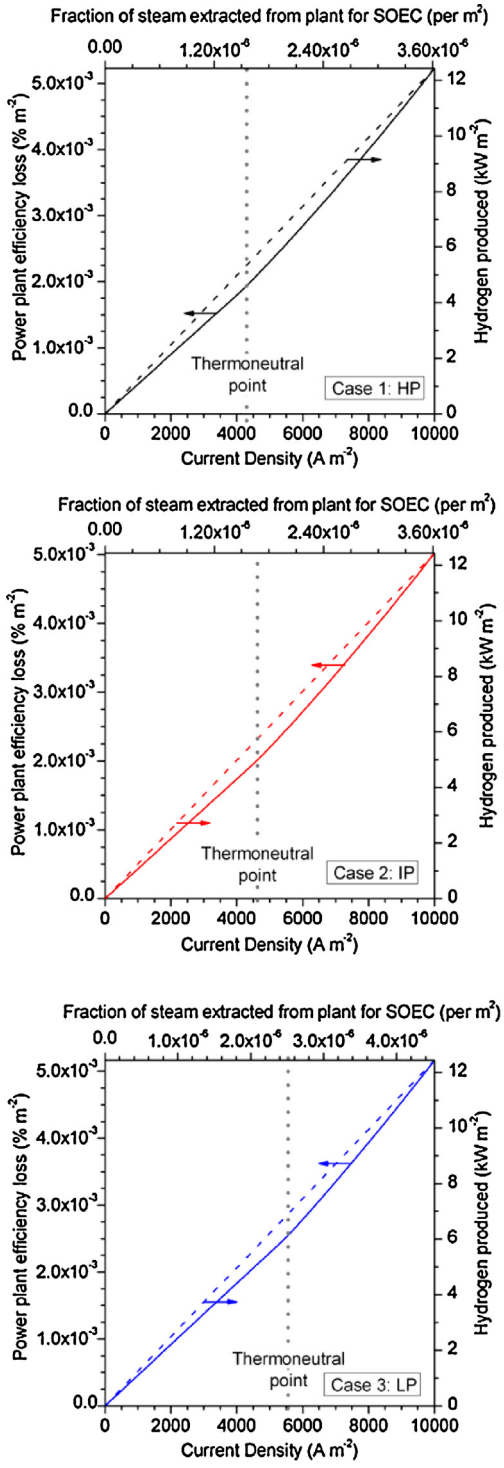

Fig. 13 – The loss of power plant efficiency (left axis) and associated hydrogen production (right axis) vs current density and associated fraction of steam extracted from the plant; for an integrated system based on Cases 1–3.

Depending on the operating point, a number of benefits and disadvantages can be noted. Generally, the thermoneutral point can allow a stable current density to meet the criteria needed for electrolysis and ensuring overpotentials are kept to a minimum. However, operating at higher current densities than the thermoneutral point may allow the heat produced to be integrated; as a result, reducing the electricity requirement of the plant for heating the steam. For a system operating at larger current densities, a suitable control strategy is needed to ensure that the material constraints of the SOEC are met.

The constraints of the materials and SOEC designs currently available are important factors when deciding on an optimum point for steam extraction from the plant. The steam extracted from Cases 1, 2 and 3 are at pressures of 250, 46 and 0.05 atm, respectively; pressurised SOEC systems to date, have been tested in the regions of 46 atm; therefore, IP conditions (Case 2) are expected to be a suitable practical option (O'Brien et al., 2010). Further benefits of Case 2 include the extent of efficiency loss from the plant not being as high as Case 1 for an almost equivalent H_2 output. Case 3 shows poor efficiencies and hydrogen output compared with Cases 1 and 2 and is therefore not considered the best option. Based on the current state of SOEC technologies, results suggest that using steam extracted from just before the IP turbine can provide suitable heat, steam and pressure to provide an efficient and productive system.

These results suggest that that integration of SOECs with power plants requires further consideration. The key to assessing the efficacy of the approach will be to consider the economics of operation over time-varying power demand profile of a power station and the value of the hydrogen produced from an energy storage and raw commodity perspective, as well as the capital cost of the SOEC, which is not known with any certainty at present. This is beyond the scope of this study; however, future work will consider an optimised system taking into consideration heat integration of the system as well as the factors influencing the economics of hydrogen production in such a system.

To ensure that the most can be made from both the plant and SOEC without restricting the day-to-day operation of the plant, the time of day that the SOECs are operational is key. In general, the plant's energy output drops significantly at night due to low energy demand and therefore turndown of up to 50% occurs (Drbal et al., 2005). Extracting the steam at night and producing hydrogen during this period allows a way of producing alternative fuels or using hydrogen as a storage vector. Furthermore, the pure oxygen produced at the anode enables the possibility of improving boiler performance and reducing harmful gas by-products through oxy-fuel operation (White et al., 2009; Kather and Kownatzki, 2011; Rehfeldt et al., 2011; Wang et al., 2012).

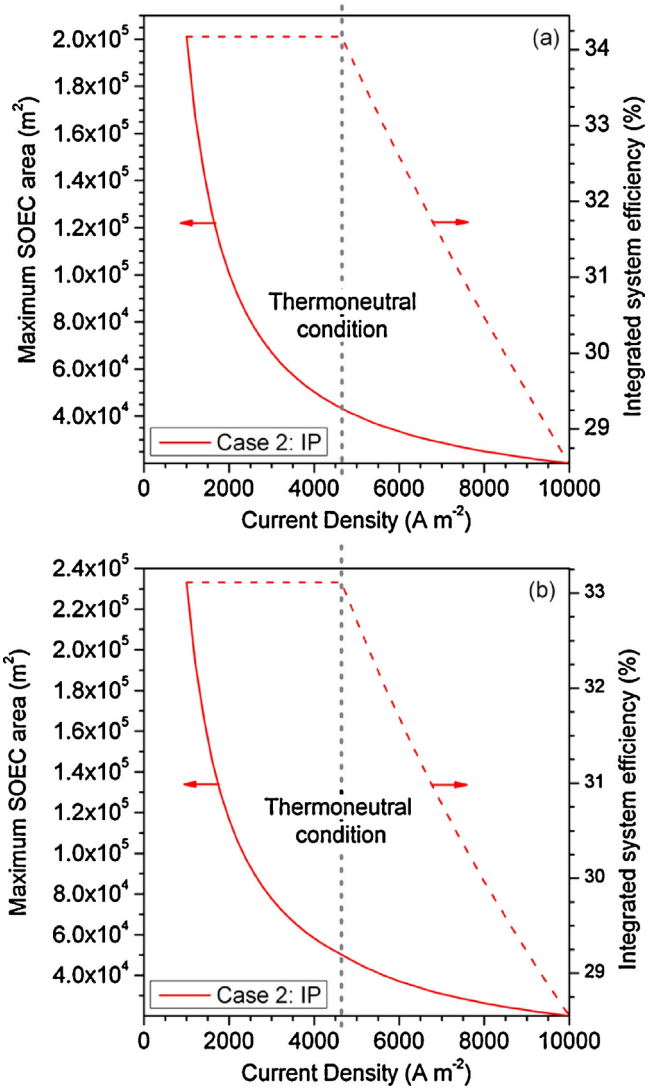

Fig. 14 – The maximum SOEC area and associated integrated system efficiency with varying current densities from Case 2: IP at (a) with a constant steam extraction of 7%; (b) a scenario where the plant is producing hydrogen only, i.e. zero electrical output to the grid.

Eq. (51) represents the overall efficiency of the integrated system ($Efficiency_{integrated}$):

$$Efficiency_{integrated} = \frac{P_{H_2}(i, A_{tot}) + P_{pp}(i, A_{tot})}{P_{input}} \times 100 \quad (51)$$

The efficiency takes into account the power produced by hydrogen (P_{H_2}) and the power which is produced from the plant once a fraction has been extracted for electrolysis (P_{pp}) as a function of current density and total area (A_{tot}) of the SOEC. P_{input} represents the chemical energy input to the system, in this case by the coal feed. Both the electrical power and heat required are taken into account in P_{pp}.

An example of a sized integrated system for a 350 MW_e power station is shown in Fig. 14. The sizing of the SOEC was carried out at each operating condition in isolation assuming 80% utilisation of steam for Case 2. The thermoneutral condition is again based on the operating condition where the heat from the overpotentials and Joule heating is equal to the energy required for heating steam and for the reaction. Fig. 14(a) shows that for a constant amount of steam extraction of 7% from the steam cycle, the SOEC area required decreases in an exponential manner. A maximum possible SOEC area is shown as for a given current density, increasing the area any further would require more steam to be extracted from the plant for a given utilisation, which would mean that the available electrical energy from the plant is insufficient to operate the SOECs. A steam extraction of 7% was chosen as this is the maximum extraction possible for the largest current density considered (10,000 A m^{-2}). The system efficiency remains constant at 34.2% before the thermoneutral point as all of the heat produced by the overpotentials is being used to raise the temperature of the extracted steam. However, after the thermoneutral condition, the heat produced is in excess and not being used effectively to contribute to the efficiency of the system, as defined by Eq. (51). To minimise efficiency fade after the thermoneutral point, the heat available from the hydrogen product stream needs to be utilised. Options are available for the heat to be used, such as to reduce electrical demands from the SOEC through heating steam or in other parts of the plant.

Another option is to use the whole plant for making hydrogen (Fig. 14(b)), such that there is no electrical energy sent to the grid (i.e. all of the electricity generated by the power plant is consumed in generating hydrogen). Once again, the analysis considered an individual design for each operating condition. However, this results in an overall system efficiency of 33.1% before the thermoneutral condition. After the thermoneutral condition, further reduction in the system efficiency is due to changes in the steam and electrical energy requirements.

In both cases shown in Fig. 14, the constant efficiency before the thermoneutral point is due to the area of the SOEC being sized for each current density and therefore is considered in isolation at each current density on the graphs. The amount of steam extracted from the plant has been calculated and remains the same by changing the SOEC area. Varying the SOEC area at a particular current density results in a change in the steam required to meet the assumed 80% utilisation.

As the amount of steam extracted remains the same, the energy required to heat the steam to the SOEC operating temperature is also constant and therefore, the power extracted from the plant to heat the steam is constant. The power to meet SOEC operating conditions vary at each current density; as the current density increases, the power needed to operate the SOEC also increases. The heat energy needed for the electrolysis process decreases as overpotentials increase with current density.

The overall power extracted from the plant before the thermoneutral point is used for producing hydrogen. After this point, power (above the required amount) is extracted from the plant to meet the current density requirements and any excess heat produced by the SOEC has not been used and therefore accounts for the loss of integrated system efficiency.

After the thermoneutral condition, the heat produced is in excess and not being used effectively to contribute to the efficiency of the system, as defined by Eq. (51). To minimise efficiency fade after the thermoneutral point, the heat available from the hydrogen product stream needs to be utilised. Options are available for the heat to be used, such as to reduce electrical demands from the SOEC through heating steam or in other parts of the plant such as preheating air to the combustor or as part of heat exchangers.

Without considering heat integration options, the thermoneutral condition represents a sensible operating point for the electrolyser, allowing a trade-off between electrolyser size and overall system efficiency. Therefore, at 4644 A m^{-2}, 250 MW (7500 kg h^{-1}) and 290 MW (8500 kg h^{-1}) of H_2 (LHV)

can be produced with SOECs sized at 43,300 and 50,100 m^2 for scenarios of 7% steam extraction and a purely H_2 production plant, respectively. Studies in literature for integrated systems with nuclear plants have also indicated that SOECs of this scale are necessary; for example, around 9×10^5 m^2 (Sohal et al., 2008).

7. Conclusions

Integrating SOECs with power plants have shown a significant improvement in SOEC efficiency compared with stand-alone SOECs, with improvements of around 25% possible at practical current densities. This shows that a large proportion of efficiency loss is due to conditioning steam to have the required thermal energy content. The thermoneutral point is shown to be a fundamental factor influencing both the design and operation, and hence the SOEC efficiency.

In the absence of a full trade-off analysis that considers capital cost and operational expense, the system thermoneutral point represents a first-order approximation as a suitable design point. Although an integrated system shows a loss in efficiency compared with the power plant alone, if used during times of low electricity demand, the economics may nevertheless still be favourable.

Notation

Parameters and variables

A_i, B_i, C_i, D_i	thermodynamic constants
A_{tot}	total area of SOEC (m^2)
b_d	constants for calculating dynamic viscosity
B_g	flow permeability (m^2)
C_i	concentration of component I (mol m^{-3})
C_p	heat capacity (J kg^{-1} K^{-1})
ΔC_p°	change in specific heat capacity (J mol^{-1} K^{-1})
$D_{Aeffave}$	average effective diffusivity (m^2 s^{-1})
D_{Aeffi}	effective diffusivity of a component i (m^2 s^{-1})
$D_{i1–i2}$	molecular diffusion of a binary mixture (m^2 s^{-1})
D_{ki}	Knudsen diffusivity of component i (m^2 s^{-1})
e	electron charge
E	potential difference (V)
E_0	open circuit potential (V)
$E_{act,tot}$	total activation overpotential (V)
$E_{conc,anode}$	concentration overpotential at anode (V)
$E_{conc,cathode}$	concentration overpotential at cathode (V)
$E_{conc,tot}$	total concentration overpotentials (V)
E_{ohm}	ohmic overpotential (V)
E_{op}	operating potential (V)
$E_{overpot}$	total overpotentials (V)
E_{tn}	thermoneutral voltage (V)
E_{rev}	reversible potential (V)
Efficiency	efficiency of the electrolyser or system (%)
$Efficiency_{Integrated}$	efficiency of an integrated system (%)
F	Faraday's constant (C mol^{-1})
ΔG	Gibbs free energy change (J mol^{-1})
ΔG_0°	Gibbs free energy at standard conditions (J mol^{-1})
ΔH	enthalpy change (J mol^{-1})
ΔH_0°	enthalpy at standard conditions (J mol^{-1})
i	current density (A m^{-2})
$i_{0,x}$	exchange current density of cathode and anode (A m^{-2})
J^*	diffusion flux (mol s^{-1} m^{-2})
k_B	Boltzmann constant
$\dot{m}_i$	mass flow rate of component i (kg s^{-1})
MW_i	molecular weight for component i (g mol^{-1})
n	number of electrons
$\dot{N}_i$	molar flow rate of component i (mol s^{-1} m^{-1})
N_A	Avogadro's number
P	operating pressure (atm)
p_i	partial pressure of component i (atm)
P_{input}	chemical energy input to the system (W)
P_{H_2}	energy produced by hydrogen (W)
P_{PP}	energy of the plant after extraction for SOEC use (W)
Q	heat energy (J mol^{-1})
$\dot{Q}_{electrolysis}$	heat required for electrolysis (W m^{-2})
$\dot{Q}_{overpotential}$	heat produced by overpotentials (W m^{-2})
$\dot{Q}_{reaction}$	heat required by reaction (W m^{-2})
$\dot{Q}_{steam}$	heat required for steam production (W m^{-2})
$\dot{Q}_{total}$	total heat requirement (W m^{-2})
q	charge
R	universal gas constant (J mol^{-1} K^{-1})
r_p	pore radius (m)
S_A	surface area of electrode (cm^2 g^{-1})
ΔS	entropy change (J mol^{-1})
T	operating temperature (K)
t	T/T_0 ($T_0 = 298.15$ K)
T_{feed}	steam/water feed temperature (K)
W_{elec}	electrical work (J mol^{-1})

Greek letters

α_i	activity of each component i
δ_i	collision diameter for component i (Å)
$\delta_{i1–i2}$	collision diameter for binary mixture (Å)
ε	porosity of electrode
$\frac{\varepsilon_{ki}}{k_B}$	characteristic energy (K)
μ	dynamic viscosity (Pa s)
υ_i	stoichiometry of components i
υ^*	molar average velocity (m s^{-1})
$\Omega_{Di1–i2}$	collision integral for binary mixture
ρ_B	bulk density (g cm^3)
σ_x	conductivity of cathode, electrolyte, anode (Ω^{-1} m^{-1})
τ_x	thickness of cathode, electrolyte, anode (m)
ξ	tortuosity

Subscripts

H_2O	water/steam
H_2	hydrogen
O_2	oxygen
i	for a given component
x	relates to cathode, anode and electrolyte

Superscripts

0	initial condition
TPB	at the three phase boundary

References

Aguiar, P., Adjiman, C.S., Brandon, N.P., 2004. Anode-supported intermediate temperature direct internal reforming solid oxide fuel cell. I: Model-based steady-state performance. J. Power Sources 138, 120–136.

Aruna, S.T., Muthuraman, M., Patil, K.C., 1998. Synthesis and properties of Ni–YSZ cermet: anode material for solid oxide fuel cells. Solid State Ionics 111, 45–51.

Baek, S.S., Lee, N., Kim, B.K., Chang, H., Song, S.J., Park, J.Y., 2012. Addition effects of erbia-stabilized bismuth oxide on ceria-based carbonate composite electrolytes for intermediate

temperature-solid oxide fuel cells. Int. J. Hydrogen Energy 37, 16823–16834.
Beér, J.M., 2007. High efficiency electric power generation: the environmental role. Prog. Energy Combust. Sci. 33, 107–134.
Bilgen, E., 2001. Solar hydrogen from photovoltaic-electrolyzer systems. Energy Convers. Manag. 42, 1047–1057.
2012. BM Reports, http://www.bmreports.com/bsp/bsp_home.htm (accessed 08.08.13).
Bo, Y., Wenqiang, Z., Jingming, X., Jing, C., 2010. Status and research of highly efficient hydrogen production through high temperature steam electrolysis at INET. Int. J. Hydrogen Energy 35, 2829–2835.
Brett, D.J.L., Atkinson, A., Brandon, N.P., Skinner, S.J., 2008. Intermediate temperature solid oxide fuel cells. Chem. Soc. Rev. 37, 1568–1578.
Brisse, A., Schefold, J., Zahid, M., 2008. High temperature water electrolysis in solid oxide cells. Int. J. Hydrogen Energy 33, 5375–5382.
Cai, Q., Luna-Ortiz, E., Adjiman, C.S., Brandon, N.P., 2012. The effects of operating conditions on the performance of a solid oxide steam electrolyser: a model-based study. Fuel Cells 10, 1114–1128.
Chalmers, H., Lucquiaud, M., Gibbins, J., Leach, M., 2009. Flexible operation of coal fired power plants with postcombustion capture of carbon dioxide. J. Environ. Eng. 135, 449–458.
Chan, S.H., Khor, K.A., Xia, Z.T., 2001. A complete polarization model of a solid oxide fuel cell and its sensitivity to the change of cell component thickness. J. Power Sources 93, 130–140.
Chan, S.H., Xia, Z.T., 2002. Polarization effects in electrolyte/electrode-supported solid oxide fuel cells. J. Appl. Electrochem. 32, 339–347.
Chemstation™, 2008. CHEMCAD Version 6.0.
Choi, Y.G., Park, J.Y., Son, J.W., Lee, J.H., Je, H.J., Kim, B.K., Lee, H.W., Yoon, K.J., 2013. Ceria-based electrolyte reinforced by sol–gel technique for intermediate-temperature solid oxide fuel cells. Int. J. Hydrogen Energy 38, 9867–9872.
Clarke, R.E., Giddey, S., Ciacchi, F.T., Badwal, S.P.S., Paul, B., Andrews, J., 2009. Direct coupling of an electrolyser to a solar PV system for generating hydrogen. Int. J. Hydrogen Energy 34, 2531–2542.
Drbal, L., Boston, P.G., Westra, K.L., Erickson, R.B., 2005. Power Plant Engineering. CBS Publishers.
2009. EIA Country Analysis Briefs, China. US Energy Information Administration.
Fujiwara, S., Kasai, S., Yamauchi, H., Yamada, K., Makino, S., Matsunaga, K., Yoshino, M., Kameda, T., Ogawa, T., Momma, S., Hoashi, E., 2008. Hydrogen production by high temperature electrolysis with nuclear reactor. Prog. Nucl. Energy 50, 422–426.
Geankoplis, C.J., 1972. Mass Transport Phenomena. Holt, Rinehart and Winston, Inc.
Gupta, R.B. (Ed.), 2008. Hydrogen Fuel, Production, Transport and Storage. CRC Press.
Hernández-Pacheco, E., Singh, D., Hutton, P.N., Patel, N., Mann, M.D., 2004. A macro-level model for determining the performance characteristics of solid oxide fuel cells. J. Power Sources 138, 174–186.
Herring, S., 2006. Laboratory-Scale High Temperature Electrolysis System. http://www.hydrogen.energy.gov/pdfs/review06/pd_17_herring.pdf (accessed 21.08.10).
Huang, J., Xie, F., Wang, C., Mao, Z., 2012. Development of solid oxide fuel cell materials for intermediate-to-low temperature operation. Int. J. Hydrogen Energy 37, 877–883.
2011. International Energy Outlook. Department of Energy, U.S. Energy Information Administration.
Jasinski, P., Suzuki, T., Dogan, F., Anderson, H.U., 2004. Impedance spectroscopy of single chamber SOFC. Solid State Ionics 175, 35–38.
Jensen, S.H., Sun, X., Ebbesen, S.D., Knibbe, R., Mogensen, M., 2010. Hydrogen and synthetic fuel production using pressurized solid oxide electrolysis cells. Int. J. Hydrogen Energy 35, 9544–9549.
Jeon, D.H., Nam, J.H., Kim, C.J., 2006. Microstructural optimization of anode-supported solid oxide fuel cells by a comprehensive microscale model. J. Electrochem. Soc. 153, A406–A417.
Kakade, M.B., Ramanathan, S., Das, D., 2011. Gel-combustion, characterization and processing of porous Ni–YSZ cermet for anodes of solid oxide fuel cells (SOFCs). Ceram. Int. 37, 195–200.
Kather, A., Kownatzki, S., 2011. Assessment of the different parameters affecting the CO_2 purity from coal fired oxyfuel process. Int. J. Greenhouse Gas Control 5, S204–S209.
Kim, S.D., Seo, D.W., Dorai, A.K., Woo, S.K., 2013. The effect of gas compositions on the performance and durability of solid oxide electrolysis cells. Int. J. Hydrogen Energy 38, 6569–6576.
Kim-Lohsoontorn, P., Kim, Y.M., Laosiripojana, N., Bae, J., 2011a. Gadolinium doped ceria-impregnated nickel–yttria stabilised zirconia cathode for solid oxide electrolysis cell. Int. J. Hydrogen Energy 36, 9420–9427.
Kim-Lohsoontorn, P., Bae, J., 2011b. Electrochemical performance of solid oxide electrolysis cell electrodes under high-temperature coelectrolysis of steam and carbon dioxide. J. Power Sources 196, 7161–7168.
Laurencin, J., Kane, D., Delette, G., Deseure, J., Lefebvre-Joud, F., 2011. Modelling of solid oxide steam electrolyser: impact of the operating conditions on hydrogen production. J. Power Sources 196, 2080–2093.
Leonide, A., Apel, Y., Ivers-Tiffee, E., 2009. SOFC modeling and parameter identification by means of impedance spectroscopy. ECS Trans. 19, 81–109.
Lightfoot, E.N., Stewart, W., Bird, R.B. (Eds.), 2002. Transport Phenomena. , 2nd ed. John Wiley & Sons, Inc., pp. 527–528, 866.
Liu, Z., Ding, D., Liu, M., Ding, X., Chen, D., Li, X., Xia, C., Liu, M., 2013. High-performance, ceria-based solid oxide fuel cells fabricated at low temperatures. J. Power Sources 241, 454–459.
Livermore, S.J.A., Cotton, J.W., Ormerod, R.M., 2000. Fuel reforming and electrical performance studies in intermediate temperature ceria–gadolinia-based SOFCs. J. Power Sources 86, 411–416.
Manage, M.N., Hodgson, D., Milligan, N., Simons, S.J.R., Brett, D.J.L., 2011. A techno-economic appraisal of hydrogen generation and the case for solid oxide electrolyser cells. Int. J. Hydrogen Energy 36, 5782–5796.
1999. Market-Based Advanced Coal Power Systems. US Department of Energy.
Marinsek, M., Pejovnik, S., Macek, J., 2007. Modelling of electrical properties of Ni–YSZ composites. J. Eur. Ceram. Soc. 27, 959–964.
Matsushima, T., Ohrui, H., Hirai, T., 1998. Effects of sinterability of YSZ powder and NiO content on characteristics of Ni–YSZ cermets. Solid State Ionics 111, 315–321.
Mench, M.M., 2008. Fuel Cell Engines. John Wiley & Sons, Inc.
Mougin, J., Chatroux, A., Couturier, K., Petitjean, M., Reytier, M., Gousseau, G., Lefebvre-Joud, F., 2012. High temperature steam electrolysis stack with enhanced performance and durability. Energy Proc. 29, 445–454.
Muecke, U.P., Graf, S., Rhyner, U., Gauckler, L.J., 2008. Microstructure and electrical conductivity of nanocrystalline nickel- and nickel oxide/gadolinia-doped ceria thin films. Acta Mater. 56, 677–687.
2012. Natural Gas Reference Guidelines, http://www.natural-gas.com.au/about/references.html (accessed 01.08.13).
Ni, M., Leung, M.K.H., Leung, D.Y.C., 2006. A modeling study on concentration overpotentials of a reversible solid oxide fuel cell. J. Power Sources 163, 460–466.
O'Brien, J.E., McKellar, M.G., Harvego, E.A., Stoots, C.M., 2010. High-temperature electrolysis for large-scale hydrogen and syngas production from nuclear energy – summary of system simulation and economic analyses. Int. J. Hydrogen Energy 35, 4808–4819.
Offer, G.J., Brandon, N.P., 2009. The effect of current density and temperature on the degradation of nickel cermet electrodes by carbon monoxide in solid oxide fuel cells. Chem. Eng. Sci. 64, 2291–2300.

Othman, M.H.D., Wu, Z., Droushiotis, N., Kelsall, G., Li, K., 2010. Morphological studies of macrostructure of Ni–CGO anode hollow fibres for intermediate temperature solid oxide fuel cells. J. Membr. Sci. 360, 410–417.
2009. Paiton III Power Station Report. International Power plc.
Perdikaris, N., Panopoulos, K.D., Hofmann, P., Spyrakis, S., Kakaras, E., 2010. Design and exergetic analysis of a novel carbon free tri-generation system for hydrogen, power and heat production from natural gas, based on combined solid oxide fuel and electrolyser cells. Int. J. Hydrogen Energy 35, 2446–2456.
Pérez-Coll, D., Núñez, P., Frade, J.R., Abrantes, J.C.C., 2003. Conductivity of CGO and CSO ceramics obtained from freeze-dried precursors. Electrochim. Acta 48, 1551–1557.
Petric, A., Huang, P., Tietz, F., 2000. Evaluation of La–Sr–Co–Fe–O perovskites for solid oxide fuel cells and gas separation membranes. Solid State Ionics 135, 719–725.
Pihlatie, M.H., Kaiser, A., Mogensen, M.B., 2012. Electrical conductivity of Ni–YSZ composites: variants and redox cycling. Solid State Ionics 222, 38–46.
2012. Post-2020 Energy Scenarios and Pathways to 2030. Institution of Civil Engineers.
Rehfeldt, S., Kuhr, C., Schiffer, F.P., Weckes, P., Bergins, C., 2011. First test results of oxyfuel combustion with Hitachi-DST-burner at Vattenfall-MWth Pilot Plant at Schwarze Pumpe. Energy Proc. 4, 1002–1009.
Roy, A., Watson, S., Infield, D., 2006. Comparison of electrical energy efficiency of atmospheric and high-pressure electrolysers. Int. J. Hydrogen Energy 31, 1964–1979.
Sanpasertparnich, T., Idem, R., Bolea, I., deMontigny, D., Tontiwachwuthikul, P., 2010. Integration of post-combustion capture and storage into a pulverized coal-fired power plant. Int. J. Greenhouse Gas Control 4, 499–510.
Santarelli, M., Medina, P., Cali, M., 2009. Fitting regression model and experimental validation for a high-pressure PEM electrolyzer. Int. J. Hydrogen Energy 34, 2519–2530.
Shin, Y., Park, W., Chang, J., Park, J., 2007. Evaluation of the high temperature electrolysis of steam to produce hydrogen. Int. J. Hydrogen Energy 32, 1486–1491.
Smith, J.M., Van Ness, H.C., Abbott, M.M., 2005. Introduction to Chemical Engineering Thermodynamics, 7th ed. McGraw-Hill.
Sohal, M.S., O'Brien, J.E., Stoots, C.M., McKellar, M.G., Harvego, E.A., Herring, J.S., 2008. Challenges in Generating Hydrogen by High Temperature Electrolysis Using Solid Oxide Cells. Idaho National Laboratory, U.S. Department of Energy.
Steele, B.C.H., Heinzel, A., 2001. Materials for fuel-cell technologies. Nature 414, 345–352.
Stoots, C.M., O'Brien, J.E., Condie, K.G., Hartvigsen, J.J., 2010. High-temperature electrolysis for large-scale hydrogen production from nuclear energy – experimental investigations. Int. J. Hydrogen Energy 35, 4861–4870.
2011. The Carbon Plan: Delivering Our Low Carbon Future. HM Government.
Udagawa, J., Aguiar, P., Brandon, N.P., 2007. Hydrogen production through steam electrolysis: model-based steady state performance of a cathode-supported intermediate temperature solid oxide electrolysis cell. J. Power Sources 166, 127–136.
Udagawa, J., Aguiar, P., Brandon, N.P., 2008. Hydrogen production through steam electrolysis: model-based dynamic behaviour of a cathode-supported intermediate temperature solid oxide electrolysis cell. J. Power Sources 180, 46–55.
2012. UK Greenhouse Gas Emissions, Provisional Figures and 2011 UK Greenhouse Gas Emissions, Final Figures by Fuel Type and End-User, Statistical Release. DECC.
Veranitisagul, C., Kaewvilai, A., Wattanathana, W., Koonsaeng, N., Traversa, E., Laobuthee, A., 2012. Electrolyte materials for solid oxide fuel cells derived from metal complexes: gadolinia-doped ceria. Ceram. Int. 38, 2403–2409.
Wang, C., Zhang, X., Liu, Y., Che, D., 2012. Pyrolysis and combustion characteristics of coals in oxyfuel combustion. Appl. Energy 97, 264–273.
White, V., Torrente-Murciano, L., Sturgeon, D., Chadwick, D., 2009. Purification of oxyfuel-derived CO_2. Energy Proc. 1, 399–406.
Woodruff, E.B., Lammers, H.B., Lammers, T.F., 2005. Steam Plant Operation, 4th ed. McGraw-Hill.
Yeh, S., Rubin, E.S., 2007. A centurial history of technological change and learning curves for pulverized coal-fired utility boilers. Energy 32, 1996–2005.
Zhang, H., Su, S., Chen, X., Lin, G., Chen, J., 2013. Configuration design and performance optimum analysis of a solar-driven high temperature steam electrolysis system for hydrogen production. Int. J. Hydrogen Energy 38, 4298–4307.
Zhen, Y.D., Tok, A.I.Y., Jiang, S.P., Boey, F.Y.C., 2008. Fabrication and performance of gadolinia-doped ceria-based intermediate-temperature solid oxide fuel cells. J. Power Sources 178, 69–74.
Zhou, T., Francois, B., 2009. Modeling and control design of hydrogen production process for an active hydrogen/wind hybrid power system. Int. J. Hydrogen Energy 34, 21–30.
Zhu, H., Kee, R.J., 2003. A general mathematical model for analyzing the performance of fuel-cell membrane-electrode assemblies. J. Power Sources 117, 61–74.